3-D Inversion of Helicopter Electromagnetic Data

M. Scheunert[1], M. Afanasjew[2], R.-U. Börner[1], M. Eiermann[2], O. G. Ernst[2], and K. Spitzer[1]
[1]Institute of Geophysics and Geoinformatics
[2]Institute of Numerical Analysis and Optimization
TU Bergakademie Freiberg (Germany)

SUMMARY

Helicopter electromagnetic (HEM) measurements allow to manage huge surveys in a very short time. Due to the enormous data and model sizes, laterally constrained 1-D inversion schemes for the entire survey are still state of the art, even for those parts of the survey where 3-D conductivity anomalies are expected.

We present the framework of an inversion scheme capable of revealing an anomalous three-dimensional conductivity structure in the subsurface for parts of the survey where 3-D conductivity anomalies are expected. For solving the inverse problem, we apply a straightforward Gauss-Newton method and a Tikhonov-type regularization scheme. The derived linear least squares problem is solved with Krylov subspace methods, such as LSQR, that are able to deal with the inherent ill-conditioning. We reformulate the discrete forward problem in terms of the secondary electric field, employing both finite difference and finite element methods. The resulting systems of linear equations subsequently yield expressions for the gradient and approximate Hessian of the minimization problem. Resulting from the unique transmitter-receiver relation of the HEM problem, an explicit representation of the Jacobian matrix is used. To handle the sensitivity-related quantities, a tensor-based problem formulation is exploited.

For application studies we consider a 3-D model problem as published by Siemon, Auken, and Christiansen (2009) using a finite difference discretization. We present first inversion results for synthetic data with a noise level of up to 5%.

Keywords: HEM, 3-D inversion, explicit Jacobian, FD and FE, Gauss-Newton

INTRODUCTION

To take advantage of a full 3-D inversion, restrictive approaches are required to overcome the enormous data and model sizes. An obvious way is to limit the inversion area to the size of the effective footprint of the measurement setup (Cox & Zhdanov, 2007). In contrast, our focus is on locating and extracting only those parts of an entire survey which are actually affected by a 3-D anomaly (Ullmann & Siemon, 2012). We show the concept of a full 3-D inversion scheme based on this restriction. We examine the theoretical background of effectively calculating the Jacobian matrix and demonstrate inversion results for airborne electromagnetics.

HEM FORWARD PROBLEM

When information on the background conductivity distribution is available, a secondary electric field approach seems practical. Maxwell's equations in their quasi-static approximation can therefore be expressed within a bounded domain $\Omega \in \mathbb{R}^3$ as

$$\nabla\times\nabla\times \boldsymbol{E}_{\mathrm{sec}} + \mathrm{i}\omega\mu_0\sigma\boldsymbol{E}_{\mathrm{sec}} = -\mathrm{i}\omega\mu_0\boldsymbol{j}_{\mathrm{pri}} \quad \text{in } \Omega, \qquad (1)$$

$$\boldsymbol{n}\times\boldsymbol{E}_{\mathrm{sec}} = 0 \quad \text{on } \partial\Omega, \qquad (2)$$

with

$$\boldsymbol{E} = \boldsymbol{E}_{\mathrm{pri}} + \boldsymbol{E}_{\mathrm{sec}}, \qquad (3)$$

where $\boldsymbol{j}_{\mathrm{pri}}(\boldsymbol{r}) = (\sigma(\boldsymbol{r}) - \sigma_{\mathrm{pri}}(z))\,\boldsymbol{E}_{\mathrm{pri}}(\boldsymbol{r})$ is a source current density driven by the primary electric field of a dipole source located above a stratified earth with electrical conductivity $\sigma_{\mathrm{pri}}(z)$.

After spatial discretization on a finite difference (FD) or finite element (FE) grid, the continuous boundary value problem can be transformed into a system of linear equations:

$$\boldsymbol{A}(\boldsymbol{\sigma})\,\boldsymbol{u} = \boldsymbol{b} \quad \text{with} \quad \boldsymbol{u} = \boldsymbol{u}_{\mathrm{pri}} + \boldsymbol{u}_{\mathrm{sec}}, \qquad (4)$$

$$\Downarrow$$

$$\boldsymbol{A}(\boldsymbol{\sigma})\,\boldsymbol{u}_{\mathrm{sec}} = -\boldsymbol{A}(\boldsymbol{\sigma})\,\boldsymbol{u}_{\mathrm{pri}} + \boldsymbol{A}(\boldsymbol{\sigma}_{\mathrm{pri}})\,\boldsymbol{u}_{\mathrm{pri}}, \qquad (5)$$

where $\boldsymbol{A}(\boldsymbol{\sigma}) = \boldsymbol{K} + \mathrm{i}\omega\mu_0\boldsymbol{M}(\boldsymbol{\sigma})$ is a sparse, complex-valued, symmetric, and typically large matrix.

The right-hand side of (5) contains the discretized source terms. The solution of the linear system yields the discrete secondary electric field $\boldsymbol{u}_{\mathrm{sec}}$.

HEM INVERSE PROBLEM

Generally, the spatial locations of sampled field components differ from the location of the discrete field components within the computational domain. Therefore, a *mapping* or *measurement operator* $\boldsymbol{Q}$ has to be defined yielding the total fields at the distinct receiver sites

$$\boldsymbol{d} = \boldsymbol{Q}\boldsymbol{u}. \tag{6}$$

We aim at finding a model parameter distribution, i. e., $\boldsymbol{m} = \log(\boldsymbol{\sigma})$, $\boldsymbol{m} \in \mathbb{R}^M$, such that the difference between measured data $\boldsymbol{d}^{\text{obs}}$ and predicted data from the forward solution $\boldsymbol{d}(\boldsymbol{m}) = \boldsymbol{Q}\boldsymbol{A}^{-1}(\boldsymbol{m})\,\boldsymbol{b}$ for a given model parameter set $\boldsymbol{m}$, as well as the parameter roughness are minimal:

$$\Phi(\boldsymbol{m}) = \frac{1}{2}\left\|\boldsymbol{d}^{\text{obs}} - \boldsymbol{d}(\boldsymbol{m})\right\|_2^2 + \frac{\lambda}{2}\left\|\boldsymbol{W}\left(\boldsymbol{m} - \boldsymbol{m}_{\text{ref}}\right)\right\|_2^2 \to \min_{\boldsymbol{m}}. \tag{7}$$

Applying the Gauss-Newton method, an approximation of $\boldsymbol{d}(\boldsymbol{m})$ is derived from a linear Taylor series expansion

$$\boldsymbol{d}(\boldsymbol{m}) \approx \boldsymbol{d}(\boldsymbol{m}_0) + \boldsymbol{J}(\boldsymbol{m}_0)\cdot(\boldsymbol{m} - \boldsymbol{m}_0), \tag{8}$$

where

$$\boldsymbol{m} = \boldsymbol{m}_0 + \Delta\boldsymbol{m}, \tag{9}$$

and $\boldsymbol{J}(\boldsymbol{m}) = \frac{\partial \boldsymbol{d}(\boldsymbol{m})}{\partial \boldsymbol{m}}$ denoting the partial derivatives of the data vector with respect to the model parameter $\boldsymbol{m}$. The resulting linearized least squares problem

$$\Phi(\boldsymbol{m}) = \frac{1}{2}\left\|\begin{bmatrix}\Delta\boldsymbol{d} \\ \sqrt{\lambda}\boldsymbol{W}(\boldsymbol{m}_0 - \boldsymbol{m}_{\text{ref}})\end{bmatrix} - \begin{bmatrix}\boldsymbol{J}(\boldsymbol{m}_0) \\ -\sqrt{\lambda}\boldsymbol{W}\end{bmatrix}\Delta\boldsymbol{m}\right\|_2^2 \to \min_{\boldsymbol{m}}, \tag{10}$$

with

$$\Delta\boldsymbol{d} = \boldsymbol{d}^{\text{obs}} - \boldsymbol{d}(\boldsymbol{m}_0), \tag{11}$$

can be solved for the model update $\Delta\boldsymbol{m}$ by Krylov subspace methods, such as CG or LSQR.

Sensitivity equation for secondary field approach

While using an FD or FE discretization an inherent approach for calculating the partial derivatives of the data with respect to the model parameter (sensitivities) is the so-called sensitivity equation. It exploits the capability of expressing the action of the forward operator in terms of the solution of a linear system of equations. Although the numerical forward problem is formulated in terms of the secondary field, we measure total fields in practice. Therefore, the inverse problem has to be defined with the total field $\boldsymbol{u}$ as simulated data. The derivative of the total field with respect to the model parameter $\boldsymbol{m}$ is given by:

$$\frac{\partial \boldsymbol{u}}{\partial \boldsymbol{m}} = \frac{\partial\left(\boldsymbol{A}^{-1}(\boldsymbol{m})\,\boldsymbol{b}\right)}{\partial \boldsymbol{m}}. \tag{12}$$

For

$$\boldsymbol{m} = \boldsymbol{m}_{\text{pri}} + \boldsymbol{m}_{\text{sec}}, \tag{13}$$

$$\boldsymbol{u}_{\text{pri}} = \boldsymbol{u}_{\text{pri}}(\boldsymbol{m}_{\text{pri}}), \tag{14}$$

$$\boldsymbol{u}_{\text{sec}} = \boldsymbol{u}_{\text{sec}}(\boldsymbol{m}_{\text{sec}}), \tag{15}$$

and supposing the primary field $\boldsymbol{u}_{\text{pri}}$ being excited by the total field source $\boldsymbol{b}$

$$\boldsymbol{A}(\boldsymbol{m}_{\text{pri}})\,\boldsymbol{u}_{\text{pri}} = \boldsymbol{b}, \tag{16}$$

(12) could be reformulated, using (5):

$$\begin{aligned}\frac{\partial \boldsymbol{A}(\boldsymbol{m})}{\partial \boldsymbol{m}}\boldsymbol{u}_{\text{sec}} + \boldsymbol{A}(\boldsymbol{m})\,\frac{\partial \boldsymbol{u}_{\text{sec}}}{\partial \boldsymbol{m}} &= \\ -\frac{\partial \boldsymbol{A}(\boldsymbol{m})}{\partial \boldsymbol{m}}\boldsymbol{u}_{\text{pri}} &- \boldsymbol{A}(\boldsymbol{m})\,\frac{\partial \boldsymbol{u}_{\text{pri}}}{\partial \boldsymbol{m}} \\ &+ \frac{\partial}{\partial \boldsymbol{m}}\left(\boldsymbol{A}(\boldsymbol{m}_{\text{pri}})\,\boldsymbol{u}_{\text{pri}}\right).\end{aligned} \tag{17}$$

Incorporating the measurement operator (6), this leads to the sensitivity matrix $\boldsymbol{J}$, i.e., the partial derivative of the reduced total field with respect to the model parameters

$$\begin{aligned}\boldsymbol{J}(\boldsymbol{m}) := \frac{\partial \boldsymbol{d}}{\partial \boldsymbol{m}} &= \boldsymbol{Q}\left(\frac{\partial \boldsymbol{u}_{\text{pri}}}{\partial \boldsymbol{m}} + \frac{\partial \boldsymbol{u}_{\text{sec}}}{\partial \boldsymbol{m}}\right) \\ &= -\boldsymbol{Q}\boldsymbol{A}(\boldsymbol{m})^{-1}\,\boldsymbol{L}(\boldsymbol{m}),\end{aligned} \tag{18}$$

with

$$\boldsymbol{L}(\boldsymbol{m}) = \frac{\partial \boldsymbol{b}}{\partial \boldsymbol{m}} - \frac{\partial \boldsymbol{M}(\boldsymbol{m})}{\partial \boldsymbol{m}} \times_2 \boldsymbol{u}. \tag{19}$$

$\widetilde{\boldsymbol{S}} = \frac{\partial \boldsymbol{M}}{\partial \boldsymbol{m}}$ is a three-way tensor with $[\widetilde{\boldsymbol{S}}]_{i,j,k} = S_{i,j,k}$. $\times_2$ denotes the tensor product along the second dimension of the tensor, i.e.,

$$\left[\frac{\partial \boldsymbol{M}(\boldsymbol{m})}{\partial \boldsymbol{m}} \times_2 \boldsymbol{u}\right]_{i,k} = \sum_j S_{i,j,k} u_j. \tag{20}$$

TX-RX relation in HEM

The HEM is typically organized such that only one field value has to be taken for every transmitter position and frequency. Thus, the numerical effort in calculating data for each transmitter and frequency as well as the numerical costs in providing the sensitivity can be reduced considerably. Concerning the Jacobian matrix, the cost of the explicit calculation by solving forward problems with $\boldsymbol{A}^{-1}$ is limited by the minimum number of either data values (N) or model parameters (M). The computational effort therefore can be reduced by using Krylov subspace methods that only require the solution of two forward problems ($\boldsymbol{J}\boldsymbol{x}$, and $\boldsymbol{J}^\top\boldsymbol{y}$) per source term and iteration. Other CSEM applications may combine a source with many receivers, whereas in HEM only one transmitter-receiver pair occurs at every transmitter position and frequency. Hence, assuming $N < M$, this inevitably leads to the fact that calculating the Jacobian matrix explicitly requires only half of the number of forward solves that would be required to implicitly calculate their action on vectors for a single Gauss-Newton iteration. This property is rapidly lost with an increasing number of receivers per transmitter.

Explicit calculation of the Jacobian

To reduce the computational costs of an explicit calculation of $\boldsymbol{J}$ from (18), it seems reasonable to exploit the sparsity of the measurement operator $\boldsymbol{Q}$. In fact, only C columns of $\boldsymbol{Q}$ include non-zero elements, whereas usually $C < K$ holds. The idea is to identify those non-zero columns of $\boldsymbol{Q}$ which are associated with the rows of $\boldsymbol{A}^{-1}$. This leads to reduced forms of the operator $\boldsymbol{Q}$ and the inverse $\boldsymbol{A}^{-1}$:

$$\boldsymbol{Q} \in \mathbb{R}^{N\times K} \quad \Rightarrow \quad \boldsymbol{Q}_r \in \mathbb{R}^{N\times C}, \tag{21}$$
$$\boldsymbol{A}^{-1} \in \mathbb{Q}^{K\times K} \quad \Rightarrow \quad \boldsymbol{A}_r^{-1} \in \mathbb{C}^{C\times K}. \tag{22}$$

Due to the symmetry of $\boldsymbol{A}^{-1}$ there holds

$$\boldsymbol{Q}\boldsymbol{A}^{-1} = (\boldsymbol{A}^{-1}\boldsymbol{Q}^\top)^\top \qquad \in \mathbb{C}^{N\times K}, \tag{23}$$
$$\Downarrow$$
$$\boldsymbol{Q}_r\boldsymbol{A}_r^{-1} = (\boldsymbol{A}_r^{-\top}\boldsymbol{Q}_r^\top)^\top \qquad \in \mathbb{C}^{N\times K}. \tag{24}$$

It is therefore necessary to calculate C forward problems with the corresponding unit vectors as the right-hand side:

$$\boldsymbol{A}^{-1}\boldsymbol{e}_c = \boldsymbol{A}_{r,c}^{-\top} \quad \text{where} \quad c = c_1, \ldots, c_C. \tag{25}$$

Hence, it is possible to explicitly form $\boldsymbol{Q}\boldsymbol{A}^{-1} = \boldsymbol{Q}_r\boldsymbol{A}_r^{-1}$ as well as to carry out the matrix-matrix multiplication with $-\boldsymbol{L}$ to provide the sensitivity matrix $\boldsymbol{J}$.

Moreover, the symmetry of $\boldsymbol{A}^{-1}$ can be exploited to solve N forward problems associated with the N rows of $\boldsymbol{Q}$ and the N columns of $\boldsymbol{Q}^\top$, respectively. This is especially useful when $\boldsymbol{Q}$ has more non-zero columns than rows, i.e., $C > N$.

A factorization of the system matrix $\boldsymbol{A}$ can substantially reduce the numerical effort required for the solution of systems with multiple right-hand sides.

Modeling area versus inverse area

In addition to the restriction of the solution vector, our approach utilizes a coarse inverse grid that is the starting point for an (adaptively) refined forward grid. Based on the cumulative sensitivities (footprint) of the a-priori known background conductivity, we define an *active* or *inner* area as part of the inverse parametrization where changes in $\boldsymbol{m} := \log(\boldsymbol{\sigma}_{\text{act}})$ are explicitly allowed. A projection operator $\boldsymbol{E}$ finally maps the inversion results back to the forward grid, such that

$$\boldsymbol{\sigma}(\boldsymbol{m}) = \boldsymbol{E}\boldsymbol{\sigma}_{\text{act}}(\boldsymbol{m}) + \boldsymbol{\sigma}_{\text{inact}} \qquad \in \mathbb{R}^S, \tag{26}$$

with

$$\boldsymbol{E} \qquad \in \mathbb{R}^{S\times M}, \tag{27}$$
$$\boldsymbol{\sigma}_{\text{act}}(\boldsymbol{m}) = \mathrm{e}^{\boldsymbol{m}} \qquad \in \mathbb{R}^M. \tag{28}$$

Figure 1 shows a typical parameter grid. The active area is outlined by a black box. It includes parameter cells associated with uniform colors. The parameter cells are a combination of cells of a fine forward grid. The latter is indicated by white lines.

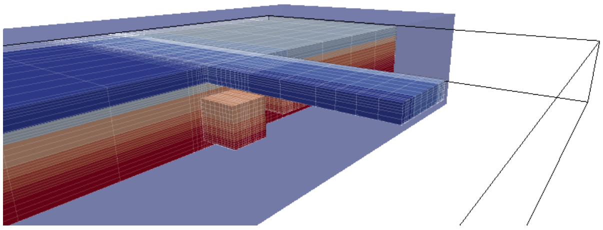

Figure 1. Section of the active inversion area.

The most important benefit from defining such an inner area is the reduction of computational costs. However, the primary field calculation involves the expensive evaluation of Hankel integrals which is extremely demanding when the forward problem is discretized on tetrahedral finite elements.

TENSOR-BASED REPRESENTATION OF THE MASS MATRIX

We apply a tensor-based implementation of the mass matrix assembly by exploiting the properties of the three-way tensor

$$\widetilde{\boldsymbol{T}} = \frac{\partial \boldsymbol{M}}{\partial \boldsymbol{\sigma}} \qquad \in \mathbb{R}^{K\times K\times S}, \tag{29}$$

that is the natural representation of the (conductivity-independent) derivative of the mass matrix. The mass matrix assembly can then be carried out by

$$\boldsymbol{M}(\boldsymbol{m}) = \widetilde{\boldsymbol{T}} \times_3 \boldsymbol{\sigma}(\boldsymbol{m}). \tag{30}$$

Another useful property of $\widetilde{\boldsymbol{T}}$ is that it provides

$$\frac{\partial \boldsymbol{M}}{\partial \boldsymbol{m}} = \widetilde{\boldsymbol{T}} \times_3 [\boldsymbol{E}\, \mathrm{diag}(\boldsymbol{\sigma}_{\text{act}})], \tag{31}$$

where

$$\frac{\partial \boldsymbol{\sigma}(\boldsymbol{m})}{\partial \boldsymbol{m}} = \boldsymbol{E}\frac{\partial \boldsymbol{\sigma}_{\text{act}}(\boldsymbol{m})}{\partial \boldsymbol{m}} \qquad \in \mathbb{R}^{S\times M}, \tag{32}$$
$$\frac{\partial \boldsymbol{\sigma}_{\text{act}}(\boldsymbol{m})}{\partial \boldsymbol{m}} = \mathrm{diag}(\boldsymbol{\sigma}_{\text{act}}) \qquad \in \mathbb{R}^{M\times M}. \tag{33}$$

For repeated multiplications with the tensor $\frac{\partial \boldsymbol{M}}{\partial \boldsymbol{m}}$ it is useful to store $\widetilde{\boldsymbol{T}} \times_3 \boldsymbol{E}$ as it is independent of $\boldsymbol{m}$, and therefore needs to be computed only once.

RESULTS

For numerical simulations and inversion studies we have defined a synthetic model (1200 m × 1800 m × 350 m) based on Siemon et al. (2009) where a rectangular block (500 m × 100 m × 20 m) is embedded in a horizontally layered half-space (Figure 2). We aim at reconstructing the conductivity distribution of $M = 13104$ cells of the active inverse area.

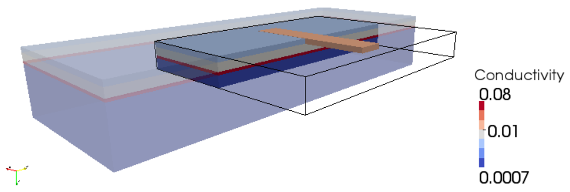

Figure 2. Sketch of the conductivity structure used for providing synthetic data.

The data points are aligned along three parallel profile lines shown in Figure 3. The inter-line spacing is 200 m. Along the profile, data is sampled every 4 m. The height of the transmitter-receiver pair above ground is $h = 30$ m. Samples of the vertical magnetic field have been collected for five frequencies. The synthetic data set comprises $N = 3765$ data points.

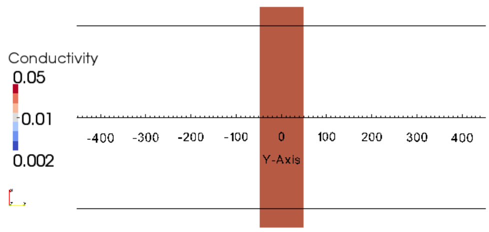

Figure 3. Top view of the anomalous conductivity structure with superimposed flight lines.

For the Tikhonov regularization we apply a combination of first and second derivatives. We include the mean background conductivity as reference model. Since the data density is not uniform, the regularization operator $\boldsymbol{W}$ may put different weights on along-profile and cross-profile model variations. Figure 4 shows a reconstruction of the conductivity distribution obtained from inversion of synthetic data contaminated with 5% Gaussian noise.

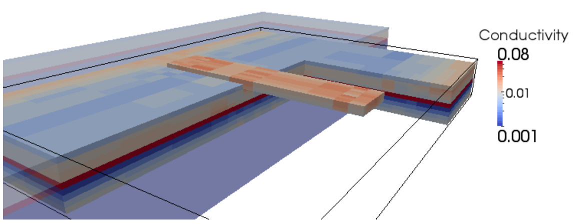

Figure 4. Conductivity distribution obtained after 12 Gauss-Newton steps.

The data fit is acceptable (Figure 5). After 12 Gauss-Newton iterations, the relative data residual has dropped to $1.3 \cdot 10^{-2}$.

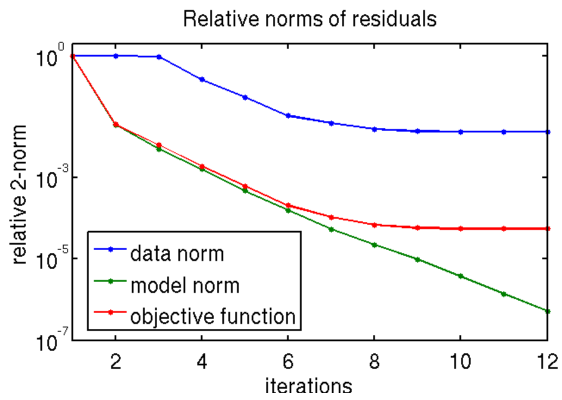

Figure 5. Convergence of data and model residuals.

OUTLOOK

Further studies will incorporate more involved weighting strategies for unstructured grids as well as the exploration of automatic updating schemes for the regularization parameter. Additionally, we aim at the investigation of case studies for real helicopter measurement data at the site “Rotschlammdeponie” near Stade, Germany.

REFERENCES

Cox, L. H., & Zhdanov, M. S. (2007). Large scale 3D inversion of HEM data using a moving footprint. In *2007 SEG Annual Meeting, September 23 - 28, 2007, San Antonio, Texas.* Society of Exploration Geophysicists.

Siemon, B., Auken, E., & Christiansen, A. (2009). Laterally constrained inversion of helicopter-borne frequency-domain electromagnetic data. *Journal of Applied Geophysics*, *67*, 259-268.

Ullmann, A., & Siemon, B. (2012). Visualisierung von Leitfähigkeitskontrasten mittels Bildbearbeitungsmethoden. In *Tagungsband zur 72. Jahrestagung der Deutschen Geophysikalischen Gesellschaft, Hamburg* (p. 121).

ACKNOWLEDGMENTS

This research has been carried out in the AIDA project funded by the German Ministry of Education and Research BMBF under the Geotechnologien Program, grant 03G0735D.